# General Disclaimer

## One or more of the Following Statements may affect this Document

- This document has been reproduced from the best copy furnished by the organizational source. It is being released in the interest of making available as much information as possible.

- This document may contain data, which exceeds the sheet parameters. It was furnished in this condition by the organizational source and is the best copy available.

- This document may contain tone-on-tone or color graphs, charts and/or pictures, which have been reproduced in black and white.

- This document is paginated as submitted by the original source.

- Portions of this document are not fully legible due to the historical nature of some of the material. However, it is the best reproduction available from the original submission.

# NASA Technical Memorandum 78725

(NASA-TM-78725) AN ANEMOMETER FOR MEASURING VELOCITIES ON THE .25 TO 4.25 M/SEC RANGE (NASA) 17 p HC A02/MF A01 CSCL 14B

N78-26407

Unclas
G3/35 21702

# AN ANEMOMETER FOR MEASURING VELOCITIES IN THE .25 TO 4.25 M/SEC RANGE

THOMAS D. CARPINI

MAY 1978


NASA
National Aeronautics and Space Administration

**Langley Research Center**
Hampton, Virginia 23665

## SUMMARY

A vane-type anemometer was developed as a secondary standard for the on-site calibration of wind velocity sensors. The instrument outputs an electrical pulse for each interruption of a light source by an eight-vane fan. The pulse rate is proportional to the fan's angular speed and linearly related to wind velocity over the range 0.25 to 4.27 m/sec.


## INTRODUCTION

In Langley's program to simulate a space laboratory, life support engineers needed a portable air-velocity secondary standard to verify, in situ, the performance of sensitive orifice meters used to measure flows of conditioned air. Air flows ranging from 0.7 to 2.83 $m^3$/min were delivered through 15.25-cm-diameter ducts to the living and working areas of the space lab. Differential pressures generated by the orifice meters were read on panel gages located in the work area and converted to flow rates. Conservation of power dictated that the air conditioning system balance be optimized for low energy consumption while still maintaining comfortable living conditions.

Normally, pitot-static probes are used as flow standards to sense the static and total head pressures as a function of velocity. The accurate measurement of airspeeds below 3 m/sec, however, is difficult to achieve with the pitot-static instrument because of the errors attending the sensing and reading of the small dynamic pressures corresponding to these velocities (0.058 cm of water column, for instance, represents 3 m/sec). The pressure errors would be prohibitive over the flow range of interest, 0.7 to 2.83 $m^3$/min (which, in a 15.25-cm duct, translates to a velocity range 0.634 to 2.54 m/sec). Furthermore, the pitot-static measurement would yield only a point velocity, which would require either a duct traverse by the probe to determine the average velocity (the desired value) or considerable trial-and-error positioning of the probe to locate the measurement point along the duct diameter where the probe would sense a velocity approximating a computed ideal average value.

An alternate instrument which proved satisfactory for measuring the low velocities and provided a reliable field standard is an electrical vane anemometer which was developed by Langley's instrument research engineers. Unique features of the anemometer are: (1) it is configured like a small, cylindrical wind-tunnel test section which could be readily inserted serially in the air ducting for calibration purposes; and (2) its output is an electrical pulse train whose frequency is directly proportional to air velocity. With the anemometer in the ducting all the flow would act upon the vanes. Since the vanes covered nearly the entire flow area, an averaging of the flow velocity was achieved.

Another more recent application for this instrument was the on-site calibration of small sensitive hot-wire anemometers used by Langley's acoustic noise reduction engineers to map the flow field of slow-moving air emanating from a subsonic noise producing jet. Radial and longitudinal distribution of the mean velocities were measured in attempts to trace the acoustic source regions of a Mach 0.67 jet used in an aircraft noise abatement program. For this calibration, the hot-wire sensors were positioned near the inlet of the anemometer and their outputs were compared to the output frequency of the anemometer over the velocity range 0.305 to 3.35 m/sec.

The purpose of this paper is to describe the design, assembly, and calibration of this anemometer and its photoelectric signal generating system which afforded remote readout capability and resulted in reduced mechanical friction, thus yielding greater sensitivity to velocities approaching zero.

## SYMBOLS

| | |
|---|---|
| C | instrument constant, such that $P = Cv$ |
| F | resultant wind force on one blade = $K\rho\omega^2 S\phi$, newtons |
| K | wind force coefficient, dependent upon the angle $\phi$ |
| P | electrical output, pulses/second |
| Q | wind torque on blades = $F \cos(\theta - \phi + \gamma)\, nr$, meter-newtons |
| S | area of one blade, $m^2$ |
| T | frictional resisting torque, meter-newtons |
| V | wind velocity, m/sec |
| n | number of blades |
| r | distance from axis of rotation to blade center of pressure, m |
| v | linear tangential velocity of blade center of pressure, m/sec |
| $\omega$ | $\sqrt{V^2 + v^2}$ = velocity of wind relative to blade, m/sec |
| $\rho$ | air density = weight per unit volume, $kg/m^3$ |
| $\theta$ | inclination of blade at rest to wind direction, degrees |
| $\phi$ | inclination of blade in motion to wind direction = effective incidence of blade, degrees |

$\gamma$ inclination of resultant wind force on blade to perpendicular to direction of relative wind, degrees

## DISCUSSION AND RESULTS

### Description of the Anemometer

The basic instrument (figs. 1, 2, and 3) consists of a light, eight-bladed, commercially built fan 9.84 cm in diameter which is mounted with oilite sleeve bearings near the center of a 35.56-cm-long cylindrical test section with polished inside walls and a diameter of 10.16 cm. The fan blades are thin trapazoidal aluminum plates, with a height of 2.54 cm and a thickness of 0.157 cm. The tops are 2.22-cm wide and slightly convex to conform to the inner wall of the anemometer. The bases are 1.6-cm wide and fastened to the ends of 0.32-cm tubular spokes such that the blades are oriented at $50^{\circ}$ to the axis of rotation and the wind direction. The inside walls are flared at each end of the test section to permit smooth flow transition from the entrance to the anemometer to the fan section and then to the exit, recalling that the anemometer was designed to fit in a 15.24-cm duct. The fan bearing assembly is held between two sets of radial struts (120 degrees apart) which are streamlined and extend from the hub to the anemometer wall. Mounted 180 degrees apart in the wall of the anemometer and at an angle of about $30^{\circ}$ from a line perpendicular to the axis of rotation are a small light source and a photodiode (figs. 1 and 3) which comprised the method for reading the output of the anemometer. Usually the fan rotation is geared to a dial indicator which displays the velocity reading. In this case, however, the clock-like mechanical movement which connects the fan to the dial was eliminated in order to reduce friction drag and extend the anemometer's low velocity range to <0.305 m/sec. With the new photoelectric sensing system, then, the output of the anemometer consisted of electrical pulses generated in the diode circuit as a result of the fan blades interrupting the light beam to the diode. The frequency of the pulses is directly related to fan rpm and thus wind velocity, and can be displayed on an electronic counter. For wind speeds greater than 1.5 m/sec, the frequency can be converted to an analog signal whose amplitude is proportional to wind velocity.

For optimum sensitivity, an attempt was made to optimize the alinement of the photoelectric elements. In order to focus the light beam directly on the photodiode, it was necessary to drill the light-mounting hole at the prescribed angle ($30^{\circ}$) in the anemometer wall. However, a perpendicular mounting hole for the photosensitive diode was found to give adequate output for the fan speeds corresponding to the velocity range of interest. The holes drilled in the wall for the photoelectric elements had no measurable effect on anemometer performance.

## Theory of Operation

The theory of the van anemometer as a velocity measuring instrument rests on the action of aerodynamic forces acting on small flat plates and was well established by Eiffel (ref. 1) and Ower (ref. 2 and 3) earlier in this century. Because of the scientific basis for its operation is well documented, only a brief discussion of the aerodynamic characteristics of flat plates as they apply here and of the anemometer's working principle will be presented.

Figure 4 shows the system of forces that acts on a flat plate when placed in an air stream. Here, AB represents an end view of the plate inclined at an angle of incidence $\phi$ to the wind direction RO. If V is the speed of the wind impinging on the plate, $\rho$ the density of the air, and S the area of the plate, the aerodynamic reactions on the plate can be reduced to a single force F acting along OQ at the center of pressure, O, Eiffel found through experiment that OQ is inclined at an angle $\gamma$ with ON (the normal to the wind direction through O) such that $\gamma$ is about equal to $\phi$ except at small values of $\phi$ (< 5 degrees) where $\gamma$ remains essentially constant as $\phi$ approaches zero degrees. The force F, then, is virtually normal to the plate, and its magnitude can be expressed by

$$F = K\rho V^2 S\phi \tag{1}$$

where K is a numerical coefficient whose value is dependent upon $\phi$.

The sketch in figure 5(a) depicts the idealized aerodynamic reactions on an anemometer blade in the absence of mechanical friction. Here AB represents one blade inclined at an angle $\theta$ to the wind direction RO. As a reference, the reader is looking down on the top edge of the blade as it rotates in a plane perpendicular to that of the page. At the instant under consideration, the blade is at the top of its circular path and moving towards the top of the page with a velocity v in the direction of ON normal to the wind direction RO. The speed of the blade will be such that the direction of the resultant velocity will be in the direction of AB. Since, in the absence of friction, there will be no retarding forces to be considered (no resultant force normal to the plane of the blade) the blade speed will simply be

$$v = V \tan \theta \tag{2}$$

In the practical case, however, where mechanical friction is taken into account, the velocity diagram becomes more complex as shown in figure 5(b). Here it is necessary to consider the aerodynamic forces acting on the blade as in Eiffel's flat plate experiment. The blade edge will still move along ON, normal to the wind direction RO, but at a lower speed v, such that the resultant (or effective) wind speed will, at steady fan motion, be inclined at an angle $\phi$ to the plane of the blade. The blade then becomes a flat plate inclined to the wind at an effective incidence angle, $\phi$ as described above in the flat plate theory. The consequence is that a resultant force F will act on the blade in the direction of OQ, at an angle $\gamma$ to ON', the normal to the relative wind direction, SO. The force component F along ON, when multiplied by the

distance that the center of pressure, O, is located away from the axis of rotation, and by the number of blades, constitutes the wind torque required to overcome the resisting torque due to friction.

The force on one blade can be written in Eiffel's terms

$$F = K\rho\omega^2 S\phi \tag{3}$$

Resolving along OS and equating wind torque, Q, to the frictional resisting torque, T, we have, for a steady motion

$$T = Fnr \cos ( \theta - \phi + \gamma ) \tag{4}$$

Substituting $K\rho\phi S(V^2 + v^2)$ for F (putting $\omega^2 = V^2 + v^2$), we have for steady motion

$$T = K\rho\phi S(V^2 + v^2)\, n\, r \cos ( \theta - \phi + \gamma ) \tag{5}$$

Also from the velocity diagram of figure 5(B)

$$v = V \tan ( \theta - \phi ) \tag{6}$$

for the linear fan tangential velocity at the center of pressure, O, from which the electrical output is

$$P = Cv = CV \tan ( \theta - \phi ) \tag{7}$$

By the foregoing, it is apparent that the rotational speed of a given set of vanes is dependent not only upon the wind speed but also the mechanical friction at the fan shaft. In the ideal case (no friction) the calibration curve is a straight line passing through the origin and whose slope is a function of the angle at which the vanes are inclined into the wind. In practice, however, friction becomes appreciable at the low speeds where $\phi$ becomes comparable with $\theta$ and v will be zero at a certain low value of V when $\phi$ is equal to $\theta$. This phenomenon is observed in the calibration curve (fig. 6).

The behavior of all well designed fan anemometers can be substantiated by the above reasoning. However, the friction torque, T, of equation (5) cannot be computed from first-hand information. If its magnitude is required, certain necessary steps must be taken after the instrument is constructed:

1. A calibration to establish the relation between v and V for several values of wind speed, V

2. Calculation of values for $\phi$ from equation (6)

3. Finding values of K from figure 7a, showing K vs $\phi$ over the $\phi$ range 0 to 45 from the work by Eiffel.

4. Finding values of $\gamma$ from figure 7B showing $\gamma$ vs $\phi$ over the $\phi$ range 0 to $40^{\circ}$, also from the work of Eiffel. The values for $\rho$ (air density), S (blade area), n (number of fan blades), and r (distance from hub to blade center of pressure) are readily obtained.

Calculation of T was not done for this work for the following reasons:

1. The fan employed in the construction of the anemometer was of classical design.

2. The calibration curve, V vs v, demonstrated the linearity and repeatability usually associated with anemometers of sound design and operation.

## Calibration

The anemometer was calibrated with the Langley gas flowmeter calibration system (ref. 4) in which precision bell-mouth sonic and subsonic nozzles are used to determine mass flow. The calibrator produces controlled air mass flow rates which are measured to better than 0.75 percent by the nozzles that have been correlated by the National Bureau of Standards. For some of these calibrations, a special ASME flow straightening section, a transition section, and a cylindrical 10.16-cm-diameter test section were attached to the exhaust of the calibrator's plenum chamber (fig. 8) so that the fan anemometer could be serially attached to the end of the 10.16 cm test section for calibration.

Three separate calibrations were made using two different measurement techniques. In the first technique, (two calibrations) the entire gas flow calibration apparatus was used with the exception of the precision sonic nozzle. Here, the average velocity was obtained by traversing the outlet of the anemometer with a small pitot-static probe whose differential pressures ($\Delta P$) were carefully measured with an MKS Baratron laboratory-type pressure system using wide-range (1000-1), capacitance-type sensors (ref. 4). The recorded pressures at each point were then converted to point velocities which were averaged for determining mean velocity. The velocity calibration range here was from 0.52 to 3.37 m/sec.

In the second technique, the main body of the calibrator was by-passed and flow was diverted through the calibrator's subsonic nozzle (fig. 8). Once steady-state flow was established at each velocity point, the mass flow through the system was measured with the subsonic nozzle located upstream of the anemometer and converted to average velocity through the anemometer based on the law of continuity, $\rho_1 A_1 V_1 = \rho_2 A_2 V_2$ (where A = area of flow passage and subscripts 1 and 2 indicate upstream and downstream conditions, respectively.) A velocity calibration range of 0.244 to 4.27 m/sec was achieved.

For both calibration techniques, the output frequency of the anemometer (fan rpm) was recorded for each standard velocity determined from the flow

nozzle or pitot-static probe. The results were plotted in figure 6 and, although some scatter is evident, there is good agreement between the two calibration sets. The calibration uncertainty for the combined data was computed to be better than $\pm$ 2 percent of full scale.

## CONCLUDING REMARKS

A low-speed electrical fan anemometer for performing on-site flow sensor calibrations was designed and built to cover a velocity range of 0.25 to 4.25 m/sec. The anemometer consisted of a small commercial fan built into a 10.16-cm diameter cylindrical housing 35.56cm long, and a sensing system whose electrical pulse output depended on the frequency of interruption of a photoelectric beam by the eight-vane fan during operation. The anemometer was calibrated over the range 0.24 to 4.27 m/sec in the Langley gas flow-meter calibration system using two independent methods for determining calibration velocities: A precision sonic nozzle and a traversing pitot-static probe. The output frequency of the anemometer (which behaved according to established anemometer theory) was plotted against each set of calibration velocities and agreement within 2 percent was achieved between the two sets.

## REFERENCES


1. Eiffel, G.: La Resistance de l'air et l'Aviation. Dunod et Pinat, Paris, 1910.

2. Ower, E.: A Low Speed Vane Anemometer. Journal of Scientific Instruments, No. 4, 1926, pages 109-112.

3. Ower, E and Pankhurst, R. C.: The Measurement of Air Flow. Pergamon Press, 1966.

4. Stump, H. P.: A Method of Calibrating Wind Velocity Sensors with a Modified Gas Flow Calibrator. NASA TMX-78707, 1978.

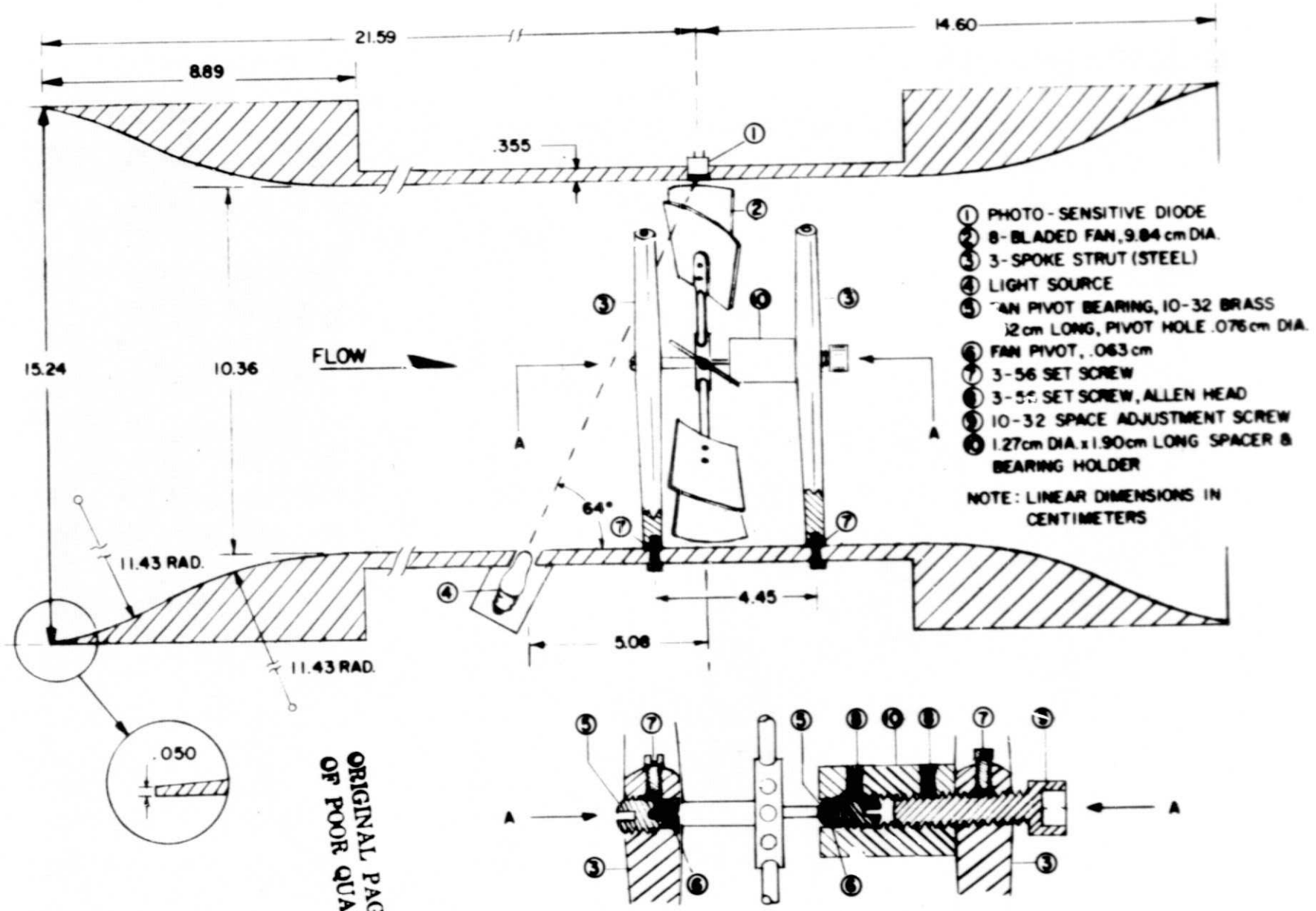


ORIGINAL PAGE IS OF POOR QUALITY

FIGURE 1- DRAWING OF ANEMOMETER

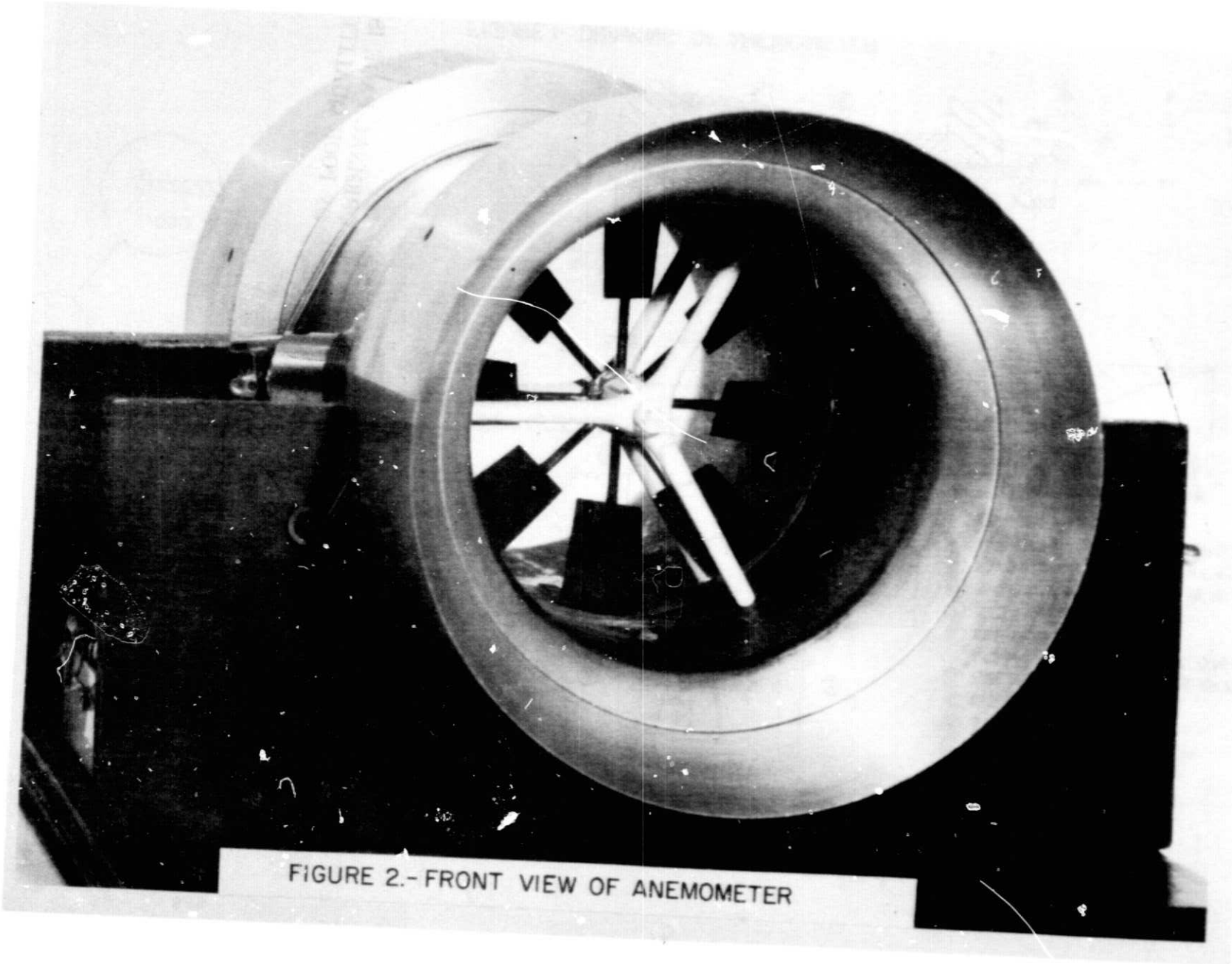

FIGURE 2.- FRONT VIEW OF ANEMOMETER

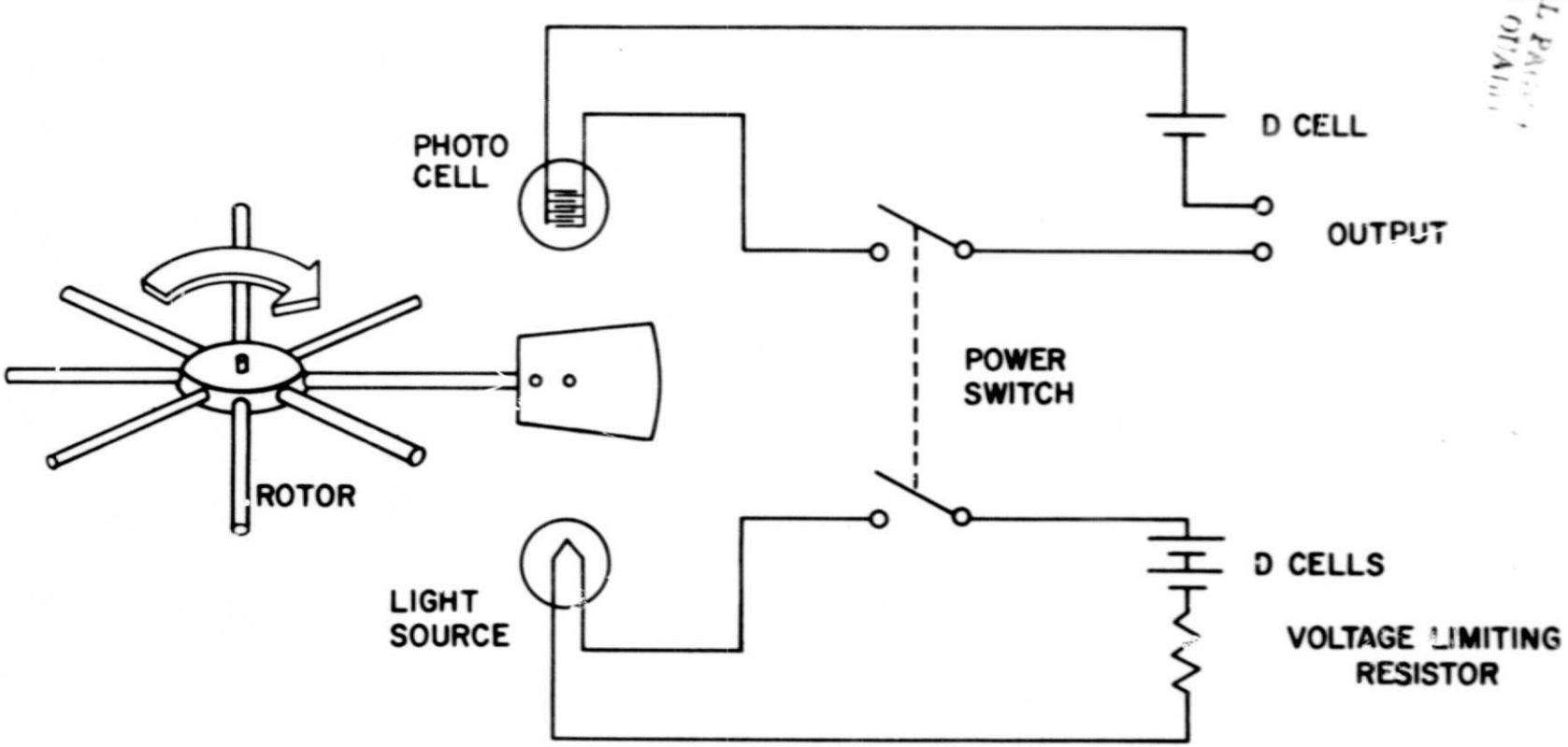


FIGURE 3.- ELECTRO-OPTICAL WIRING DIAGRAM.

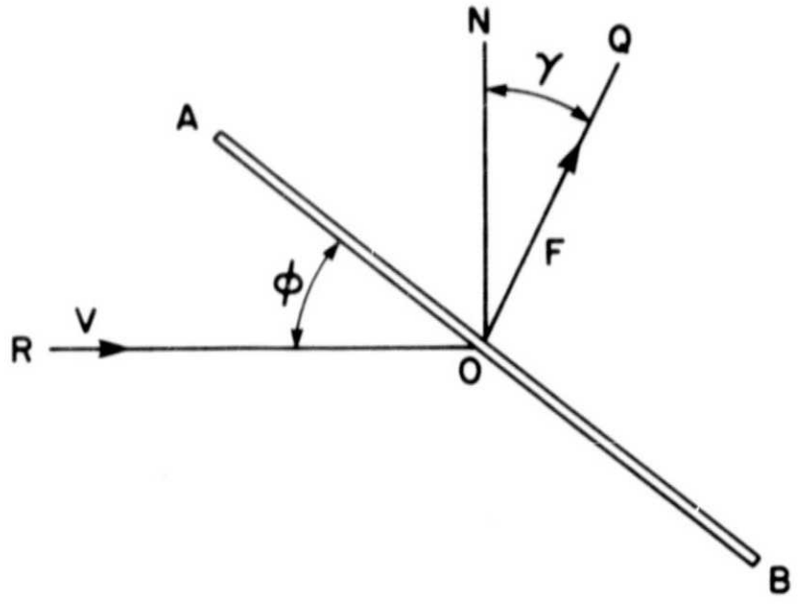


FIGURE 4.- AERODYNAMIC REACTIONS ON A FLAT PLATE.

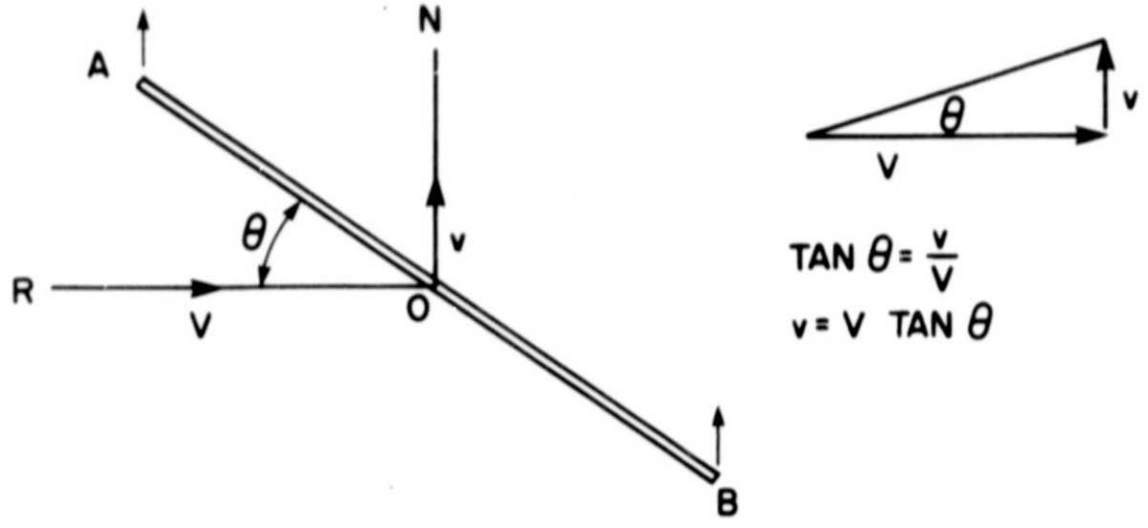


(A) IDEALIZED AERODYNAMIC REACTIONS ON AN ANEMOMETER BLADE IN THE ABSENCE OF MECHANICAL FRICTION.

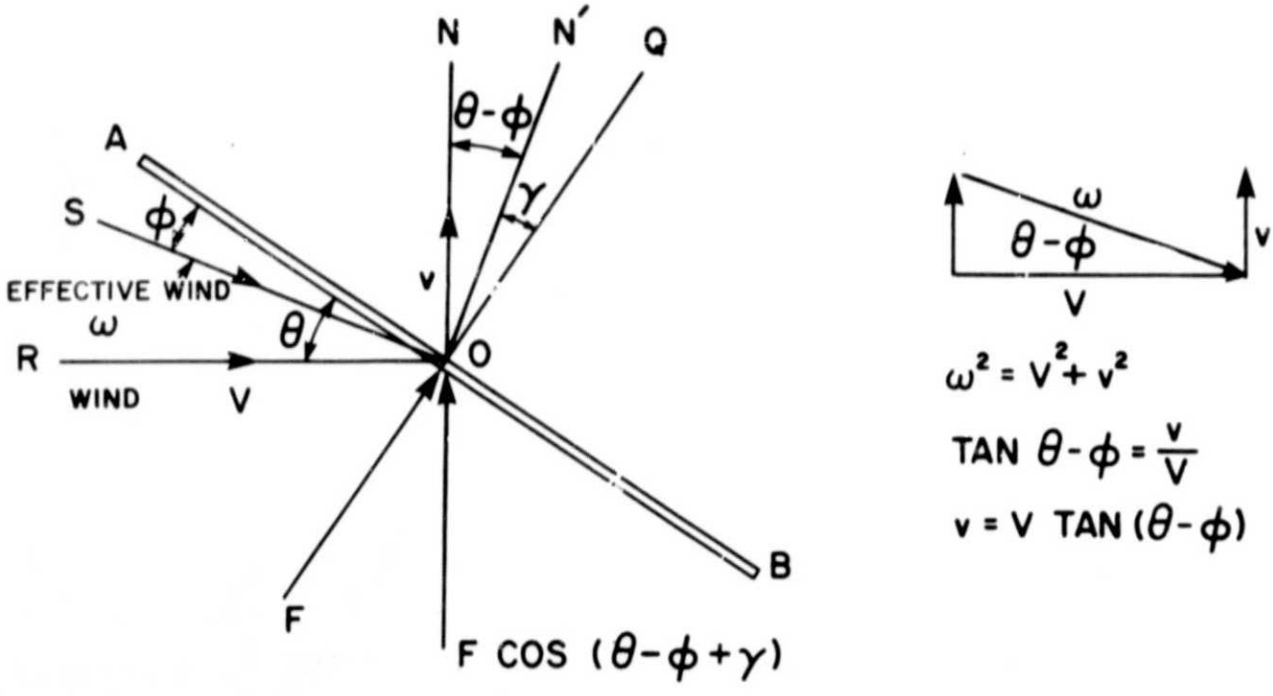


(B) WITH MECHANICAL FRICTION

FIGURE 5.- AERODYNAMIC REACTIONS ON AN ANEMOMETER BLADE.

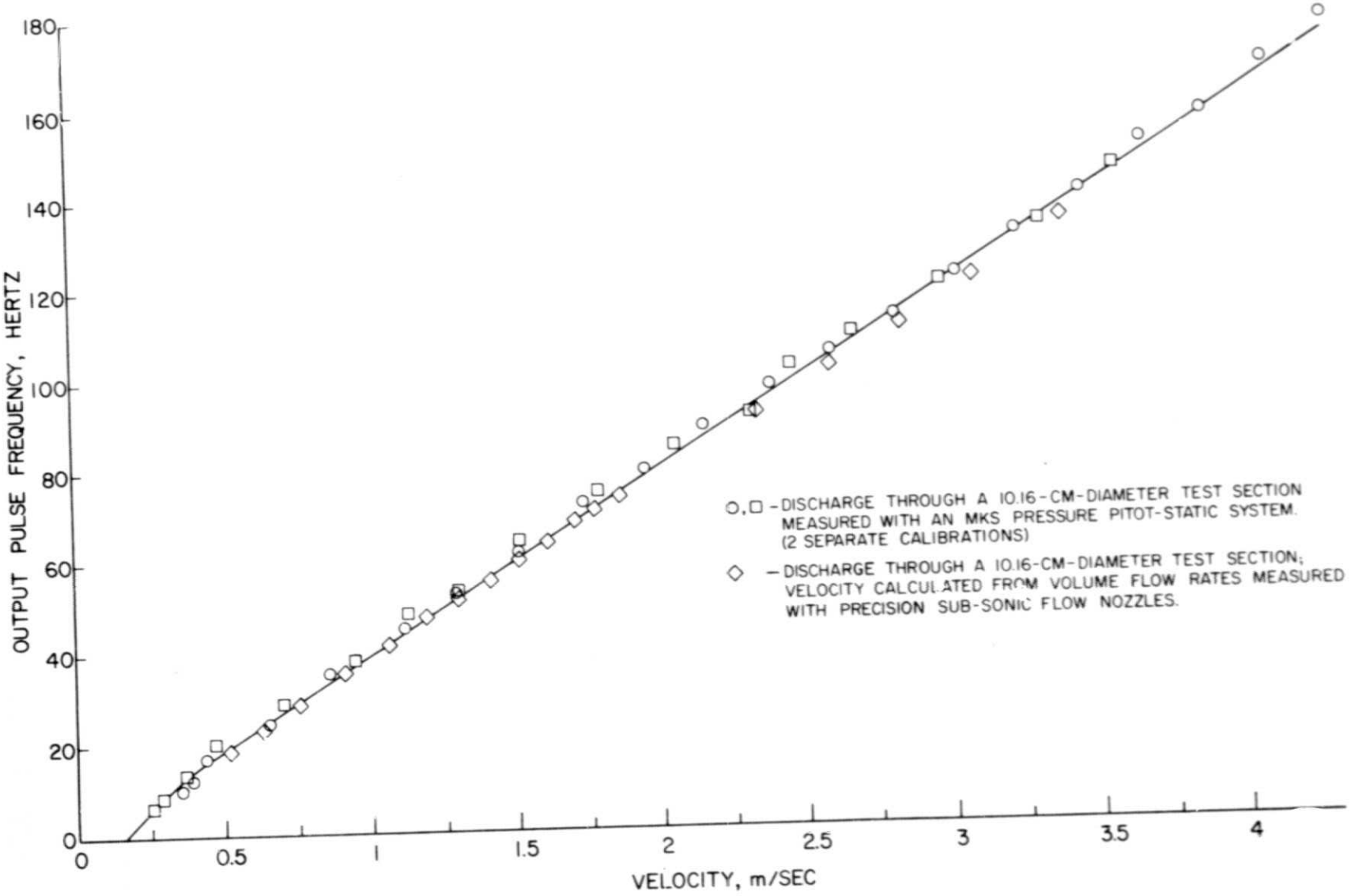


FIGURE 6. - VARIATION OF ANEMOMETER OUTPUT WITH AIR VELOCITY.

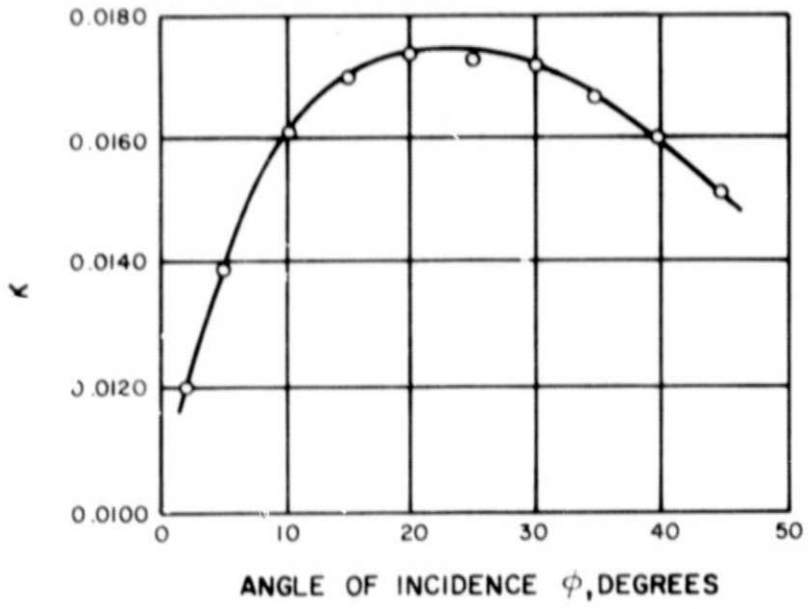


(A) AERODYNAMIC-FORCE COEFFICIENT ON A FLAT PLATE.

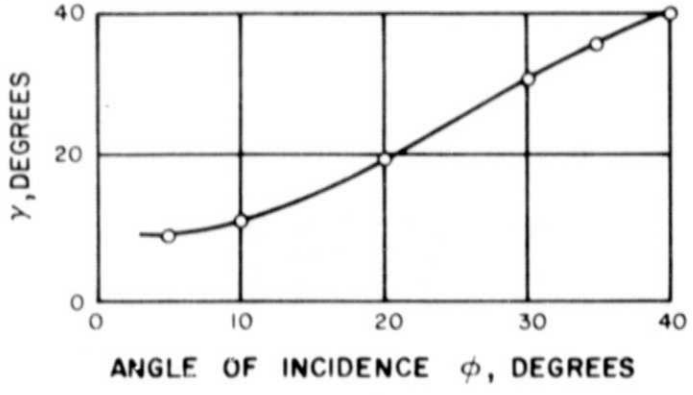


(B) ANGLE OF AERODYNAMIC REACTION ON A FLAT PLATE.

FIGURE 7. - EIFFEL'S EMPIRICAL CURVES ON THE AERODYNAMIC REACTIONS ON A FLAT PLATE.

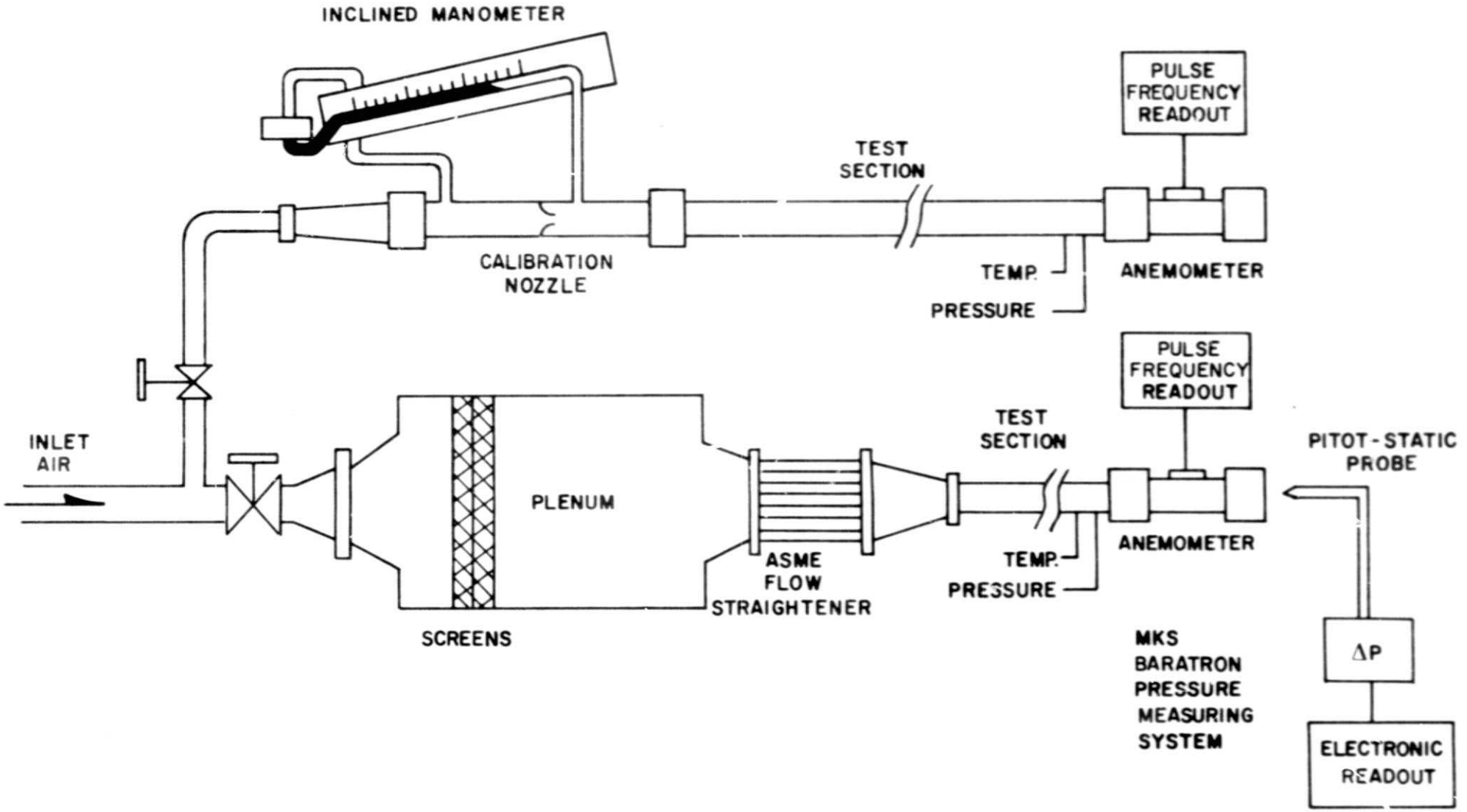


FIGURE 8.- CALIBRATION SYSTEM